Journal Title
XX(X):1–12

DOI: 10.1177/ToBeAssigned
www.sagepub.com/
SAGE

Fuel consumption and aftertreatment thermal management synergy in compression ignition engines at variable altitude and ambient temperature

José Ramón Serrano, Vicente Bermúdez, Pedro Piqueras and Bárbara Diesel

Abstract

New regulations applied to the transportation sector are widening the operation range where the pollutant emissions are evaluated. Besides ambient temperature, the driving altitude is also considered to reduce the gap between regulated and real-life emissions. The altitude effect on the engine performance is usually overcome by acting on the turbocharger control. The traditional strategy assumes to keep (or even to increase) the boost pressure, i.e. compressor pressure ratio increase, as the altitude is increased to offset the ambient density reduction, followed by the reduction of the exhaust gas recirculation to reach the targeted engine torque. However, this is done at the expense of an increase on fuel consumption and emissions. This work remarks experimentally the importance of a detailed understanding of the effects of the boost pressure and low pressure exhaust gas recirculation (LP-EGR) settings when the engine runs low partial loads at different altitudes, accounting for extreme warm and cold ambient temperatures. The experimental results allow defining and justifying clear guidelines for an optimal engine calibration. Opposite to traditional strategies, a proper calibration of the boost pressure and LP-EGR enables reductions in specific fuel consumption along with the gas temperature increase at the exhaust aftertreatment system.

Keywords

Internal combustion engine, Altitude, Ambient temperature, Fuel consumption, Thermal management, Emissions

Introduction

Increasingly tight emissions standards are being formulated by government institutions all around the world motivated by the need to reduce the health and environmental effects caused by the transportation sector[1]. Besides quantitative limits applied to regulated pollutants and the incoming consideration of additional chemical species[2], such as ammonia or methane, the regulatory framework is driving the focus to the type-approval procedures. In Europe, the current driving cycle tests performed on chassis dyno (Worldwide harmonized Light vehicles Test Cycle (WLTC)), are complemented with on-road real driving emissions (RDE) tests[3]. While WLTC comprises temperatures of -7°C, RDE cover additional boundaries and ranges concerning ambient conditions. On the one hand, the window of ambient temperature is defined from 0°C to 30°C within the moderate range and from -7 to 35°C in the extended one accounting for an additional emissions corrective factor. On the other hand, altitude is also considered to account for a more accurate control of emissions in populated areas over sea-level[4], including below 700 m in the moderate range and from this altitude to 1300 m in the extended one. The European approach is also being applied in other countries with adaptations to the singularities of every region, such as a higher temperature range (8-45°C) in India or altitude till 2400 m in China for extended ranges.

The engine performance is very sensitive to the variation of the ambient conditions, that may lead to a global negative impact on emissions and fuel consumption[5]. Ko *et al.*[6] showed a large impact of ambient temperature below 0°C on CO and NO_x emissions of a Euro 6 engine equipped with a lean NO_x trap (LNT). Although CO emission was almost duplicated at -5°C with respect to 23°C, it still was kept below the Euro 6 limits in WLTC. However, at very low ambient temperature, NO_x emission exceeded such limits after a sevenfold increase at -5°C with respect to the baseline because of the poor efficiency of the LNT. In addition, the exhaust gas recirculation (EGR) rate is usually decreased in these conditions to avoid the condensation phenomena in the LP-EGR cooler during warm-up[7] and in the mixing region with fresh air upstream of the compressor[8]. This can yet be partially can be partially balanced by using a LP-EGR cooler by-pass[9].

Luján *et al.*[5] also analysed the impact of very low ambient temperature on the CO and HC emissions of a diesel engine running WLTC tests. The engine was equipped with high pressure (HP) and LP-EGR operating with serial calibration. Both EGR systems were kept fully close till 875 s at -7°C in ambient temperature and remained closer than at 20°C in all WLTC phases. This control strategy produced an increase in engine-out NO_x and HC emissions along the whole cycle but only a relevant CO emission increase during

Universitat Politècnica de València, Spain

Corresponding author:
Pedro Piqueras, CMT-Motores Térmicos, Universitat Politècnica de València, Camino de Vera s/n, 46022 Valencia, Spain.
Email: pedpicab@mot.upv.es

the low speed WLTC phase. The results were even worse when running the New European Driving Cycle (NEDC). The penalty in fuel consumption was around 10% in both driving cycles with respect to warm ambient temperature [10]. In a snowball effect, the conversion efficiency of the diesel oxidation catalyst (DOC) was also deteriorated at -7°C by the lower exhaust temperature as well as the increase of the inhibition due to the huge peaks of emissions caused by high demanding accelerations [11]. Faria *et al.* [12] observed an increase of fuel consumption and emissions at low ambient temperature within the moderate temperature range, being gasoline engines damaged the most. Ko *et al.* [13] found the same trends in cold and warm restartings for a sample of Euro 5 and Euro 6 vehicles. Nevertheless, this study evidenced the high performance of the de-NOx techniques in state-of-the-art Euro 6 vehicles, concerning both EGR and aftertreatment system (ATS) solutions, with respect to Euro 5 counterparts.

As ambient temperature, the altitude variation, which implies different ambient pressures, also leads to relevant effects on the combustion [14], the gas exchange processes [15] and the ATS performance [16,17]. Wang *et al.* [18] found a progressive decrease in brake thermal efficiency with increasing altitude in a heavy duty diesel engine. These trends are consistent with those recently found by Giraldo and Huertas [19] in diesel buses operating at high altitude, especially for high vehicle speeds. In the same way, Szedlmayer and Kweon [14] reported a damage in indicated specific fuel consumption, reaching 8% at high altitude and high load. However, slight benefits were found at low load. In a similar way, Ramos *et al.* [20] tested a passenger car diesel engine and observed an increase in fuel consumption in extra-urban driving conditions at ~ 2300 m. In this line, Serrano *et al.* [15] reported a progressive fuel consumption penalty with increasing altitude, both in urban and, especially, extra-urban driving phases of NEDC. In gasoline engines, the results in the literature are focused on naturally aspirated engines. Zervas [21] reported a decrease in fuel consumption reaching 3.5% in NEDC, 2.6% in Fedetal Test Procedure and 6.2% in the Highway driving cycle; Wang *et al.* [22] also found a decrease in CO_2 emission as altitude increased for various naturally gasoline vehicles operating under WLTC mainly because of the intake throttle opening.

Bearing in mind the need of high EGR rates to keep low levels of NO_x emission in diesel engines, altitude operation imposes additional constraints since the engine systems tend to work closer to their mechanical and operational limits [23]. On the one hand, the combustion instabilities require to reduce the EGR rate as altitude increases [20]. In a similar way, medium engine loads demand the turbocharger protection so that the high-pressure EGR rate is decreased to provide compressor surge margin and avoid to exceed the turbine inlet temperature turbocharger speed limits [15]. With these trends, a huge penalty in NO_x emission can be obtained, as demonstrated by Ramos *et al.* [20], who reported ten times higher NO_x emission than the regulation limits for a Euro 4 diesel vehicle; Wang *et al.* [24] also observed the progressive increase of NO_x emission as well as CO and particulate matter (PM) till almost 3000 m, in agreement with the results of Serrano *et al.* till 2500 m [15].

The EGR closing in altitude operation is also justified as a way to avoid the increase of the equivalence ratio as the total mass flow across the engine intake decreases. In parallel, the turbocharger control plays an important role. Yang *et al.* [25] found that the variable geometry turbine (VGT) technology is the one providing the highest flexibility to optimise the engine response in variable altitude operation. The standard trend consists of the VGT closing to compensate the reduction in ambient density by increasing the compression ratio with respect sea-level to recover the boost pressure [26]. Although this strategy allows keeping the sea-level engine performance in a wide altitude window, the performance of turbocharged engines is deteriorated. The reason is the exhaust manifold pressure increase, which gives rise to the pumping losses and the pollutant emissions increments [4]. Recently, Wang *et al.* [27] performed a modelling study and optimisation of the steady-state calibration for fuel consumption and NO_x-PM emission minimisation at high altitude for a light-duty diesel engine from 25% in load on. Their results confirmed a positive response of gradually closing the EGR valve as the engine load increased, being more complex the determination of optimum turbine position. From low to medium speed, the turbine was very closed but slightly more open at low load. A progressive opening was obtained as the engine speed increased over 2500 rpm till 4000 rpm. However, the opening was more pronounced at high load and engine speed range compared to low engine speed case.

In this context, the purpose of this work is to identify the impact of the boosting pressure and EGR rate on the performance, emissions and exhaust thermal conditions of a Euro 6d-Temp turbocharged diesel engine working at low partial load as a function of altitude and ambient temperature. For the sake of understanding, an analysis of the parameters governing the engine response is also performed. The engine was tested under steady-state conditions in an engine test bench making use of the altitude simulator Horiba Multifunctional Efficient Dynamic Altitude Simulator (MEDAS) [28]. From the baseline engine serial calibration, the tests were performed varying the VGT and low pressure (LP-) EGR valve positions to sweep a representative range of boost pressure and EGR rate of three low load operating points of different engine speed. The parametric study covered three ambient temperatures, from -10°C to 45°C including the standard temperature (25°C) and three altitudes, namely sea-level, 1300 m and 2500 m. The results establish clear guidelines for an optimal calibration within the tested engine range with synergistic minimisation of the specific fuel consumption and maximisation of the aftertreatment inlet temperature while balancing pollutant emissions.

Materials and Methods

This study was performed in a Euro 6d-Temp passenger car diesel engine whose main characteristics are summarised in Table 1. The engine air path accounted for a variable geometry turbine (VGT), water charge air cooler and HP- and cooled LP-EGR. An aftertreatment brick composed of a DOC and a wall-flow particulate filter was located

downstream of the VGT outlet whilst the serial underfloor selective catalytic reduction system was omitted in this work.

Table 1. Main characteristics of the engine.

Engine type	Four-stroke HSDI diesel
Emissions Standards	Euro6d-Temp
Number of cylinders	4 in line
Displaced volume [cm^3]	1461
Bore [mm] × Stroke [mm]	76 × 80.5
Number of valves	2 per cylinder
Compression Ratio	15.2:1
Fuel Injection	Common-rail direct injection
Turbocharger	VGT
EGR system	HP- and cooled LP-EGR
ATS system	Closed-coupled DOC+DPF

The engine was installed in a test bench, which is schematically illustrated in Figure 1, equipped with an asynchronous dynamometer controlled by the automation system AVL PUMA Open 2. In addition, the engine intake, exhaust and sump were coupled to an altitude simulator to control the requested atmospheric boundary conditions during the engine tests[29,30]. The altitude simulator was composed of a Horiba MEDAS, which was developed at CMT-Motores Térmicos[31,32], coupled with its temperature module for an accurate control of ambient pressure, within variable altitude from sea-level to 5000 m, and temperature, which can be controlled between -15 and 45°C. The engine operation was also controlled by acting on an open engine control unit (ECU), which was available to modify the engine calibration accessing it through the ETAS INCA software. In particular, the boost pressure and the exhaust gas recirculation (EGR) rate were modified, as forward described.

The main magnitudes defining the engine and aftertreatment performance were measured. Besides engine torque and speed, the in-cylinder pressure was also measured. The air and fuel mass flows were obtained by a hot-wire anemometer and a gravimetric balance respectively. Temperature and mean pressure were monitored along the air and exhaust gas paths. The turbocharger speed was also measured to analyse the turbine and compressor performance as well as to monitor its operation out of overspeed and surge regions.

The pollutants emissions were measured by an opacimeter placed upstream of the wall-flow particulate filter and by the Horiba Mexa ONE gas analysers extracting exhaust gas samples upstream and downstream of the DOC. Since NO_x abatement was not carried in the ATS, only the engine-out emissions and the CO and HC conversion efficiency were monitored. A gas mass from the intake manifold was also sampled to measure the CO_2 concentration and determine the EGR rate along with the engine out CO_2 concentration.

Test campaign

The study was focused in low partial load engine operating conditions. Table 2 enumerates the three tested engine operating points, which ranged from 2 to 6 bar in break mean effective pressure (BMEP). The engine speed selection covered 1250 to 3000 rpm. Every operating point was evaluated at 9 different ambient boundaries. From the altitude point of view, sea-level, 1300 m, which is the maximum altitude in Euro 6d extended range, and 2500 m, which involves a global upper limit of maximum altitude in emission stardards (for example, 2400 m in China 6b), were tested. In parallel, the ambient temperature was swept from very cold conditions (-10°C) to very warm ones (45°C) with an intermediate temperature represented by the standard ambient conditions (25°C).

A parametric study was done for every operating point at every ambient condition sweeping boost pressure and EGR rate. The VGT rack was actuated to contol the boost pressure. Concerning the EGR rate, the LP-EGR was actuated since the study was performed under steady-state conditions and the engine coolant temperature reached 60°C. Therefore, the LP-EGR valve and the exhaust back-pressure valve were set to impose the target EGR rate. The study was carried out according to the following testing procedure:

1. The engine was set at every operating point condition referenced in Table 2 according to the serial ECU calibration. The fuel mass flow obtained in this condition was kept constant for the entire parametric study.
2. From the baseline point, a boost pressure sweep was performed covering an amplitude of 200 mbar. As a general trend, the baseline VGT position tended to be very closed, so that the boost pressure was decreased in steps of ~ 50 mbar. In these cases where the VGT reached fully opening condition without reaching a test range of 200 mbar, additional VGT positions closer than the baseline one were tested to have comparable boost pressure windows and sensitivity to this variable in all the parametric studies.
3. For every boost pressure considered in the previos step, the LP-EGR rate was progressively decreased up to $\sim 15\%$ in absolute value with respect to the baseline LP-EGR rate. To keep this range in the case of reaching 0% of LP-EGR rate, the baseline LP-EGR rate was increased until achieving a range of at least 15% for the study.

This procedure enabled the representation of contour maps corresponding to every magnitude of interest for different altitude and ambient temperature combinations as a function of the boost pressure and LP-EGR rate. In every contour plot, the tested operating conditions are marked by a black dot. The baseline operating point (serial calibration) is identified by a greater dot than its counterparts, in red or green colour depending on the background contour colour to be properly distinguished. For comparison proposals, some plots encompass more than one ambient condition contour map provided that there is not overlap between tested regions.

Engine performance and exhaust temperature

Figure 2 illustrates air mass flow, compressor pressure ratio and VGT position corresponding to the operating point 1250 rpm & 3 bar at 25°C in ambient temperature as a function of the altitude, boost pressure and LP-EGR rate. Comparing the boost pressure and LP-EGR ranges corresponding to every altitude (columns in Figure 2), a decrease in LP-EGR rate

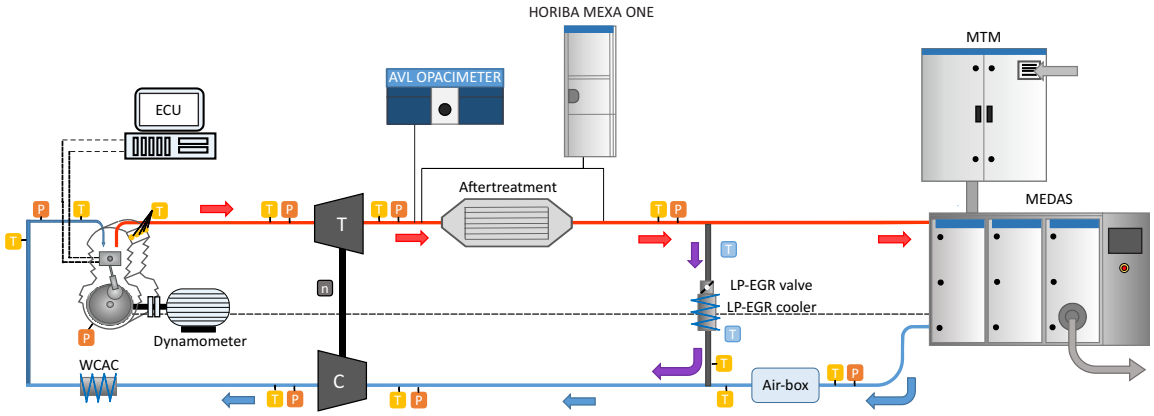

Figure 1. Scheme of the engine test bench.

Table 2. Definition of the tested operation conditions.

Operating point	Altitude [m]	Ambient temperature [°C]	WCAC outlet temperature [°C]
#A - 1250 rpm & 3 bar	0 / 1300 / 2500	-10	0
	0 / 1300 / 2500	25	28
	0 / 1300 / 2500	45	48
#B - 2000 rpm & 6 bar	0 / 1300 / 2500	-10	5
	0 / 1300 / 2500	25	29
	0 / 1300 / 2500	45	49
#C - 3000 rpm & 2 bar	0 / 1300 / 2500	-10	7
	0 / 1300 / 2500	25	35
	0 / 1300 / 2500	45	55

window was noticed as altitude increased. In parallel, the boost pressure range also decreased. However, this response was expected from the ambient pressure decrease. The results point out that the tested regions at every altitude provided the same order of magnitude regarding air mass flow. The engine actuated moving the serial calibrated point to lower LP-EGR rate progressively, but keeping the same air mass flow, i.e. the same air-to-fuel ratio, as the baseline case. However, as indicated by the coloured points in the contour plots, while the baseline LP-EGR rate was 39% at sea-level, it was decreased to 34% at 1300 m and dropped till 20% at 2500 m. The boost pressure also decreased from 1060 mbar at sea-level to 960 mbar at 1300 m and 860 mbar at 2500 m. Despite of the boost pressure decrease, the compressor pressure ratio of the baseline point was gradually increased as altitude did, closing the VGT to provide the same air mass flow as at sea-level. Therefore, the serial engine calibration maximized the LP-EGR rate to reduce the impact on NO_x emissions. To do that, the pressure ratio was increased closing the VGT to keep the same equivalence ratio as at sea-level. This target of the calibration process found its limit in the specific fuel consumption penalty.

The increase of the compressor pressure ratio and the VGT closing involved a penalty in torque and brake specific fuel consumption (BSFC), which are represented in Figure 3. The BSFC is normalized with respect to the BSFC obtained in the serial calibration condition at sea-level and 25°C. The BSFC deterioration was observed in the serial calibration points as a function of the altitude, particularly, and evidenced by the trends within the tested boost pressure and LP-EGR rate ranges at every altitude. Although the serial calibration fell into the maximum torque and minimum BSFC regions at sea-level and 1300 m, these magnitudes might be optimized at 2500 m. The main output from Figure 3 was that the best strategy to minimize the fuel consumption in the low load operating point would consist of the VGT opening to reduce the boost pressure. This might be done regardless of the LP-EGR rate, so that to find the optimal balance between equivalence ratio and engine-out NO_x emission would be still possible.

Figure 4 depicts the VGT expansion ratio as well as inlet and outlet temperatures at every altitude for 1250 rpm & 3 bar. As in the previous variables, the LP-EGR rate played a negligible role being the boost pressure the governing parameter. The increase of the compressor pressure ratio required the VGT expansion increase induced by the VGT closing. Accordingly, the VGT expansion ratio behaved as the compressor pressure ratio, increasing as the altitude increased both within the tested range and, specifically, in the baseline operating point. Regarding temperature, the VGT inlet temperature slightly increased from sea-level to 1300 m, with a more pronounced increase at 2500 m due to the lower amount of exhaust mass flow. These differences in inlet temperature as a function of altitude were also present in VGT outlet temperature, but with a different pattern. On the one hand, the maximum VGT inlet temperatures were obtained for the extreme VGT positions. The highest VGT inlet temperatures were caused by the high pressure in VGT fully closed condition and by the lower air mass flow (higher equivalence ratio) as the VGT was opened.

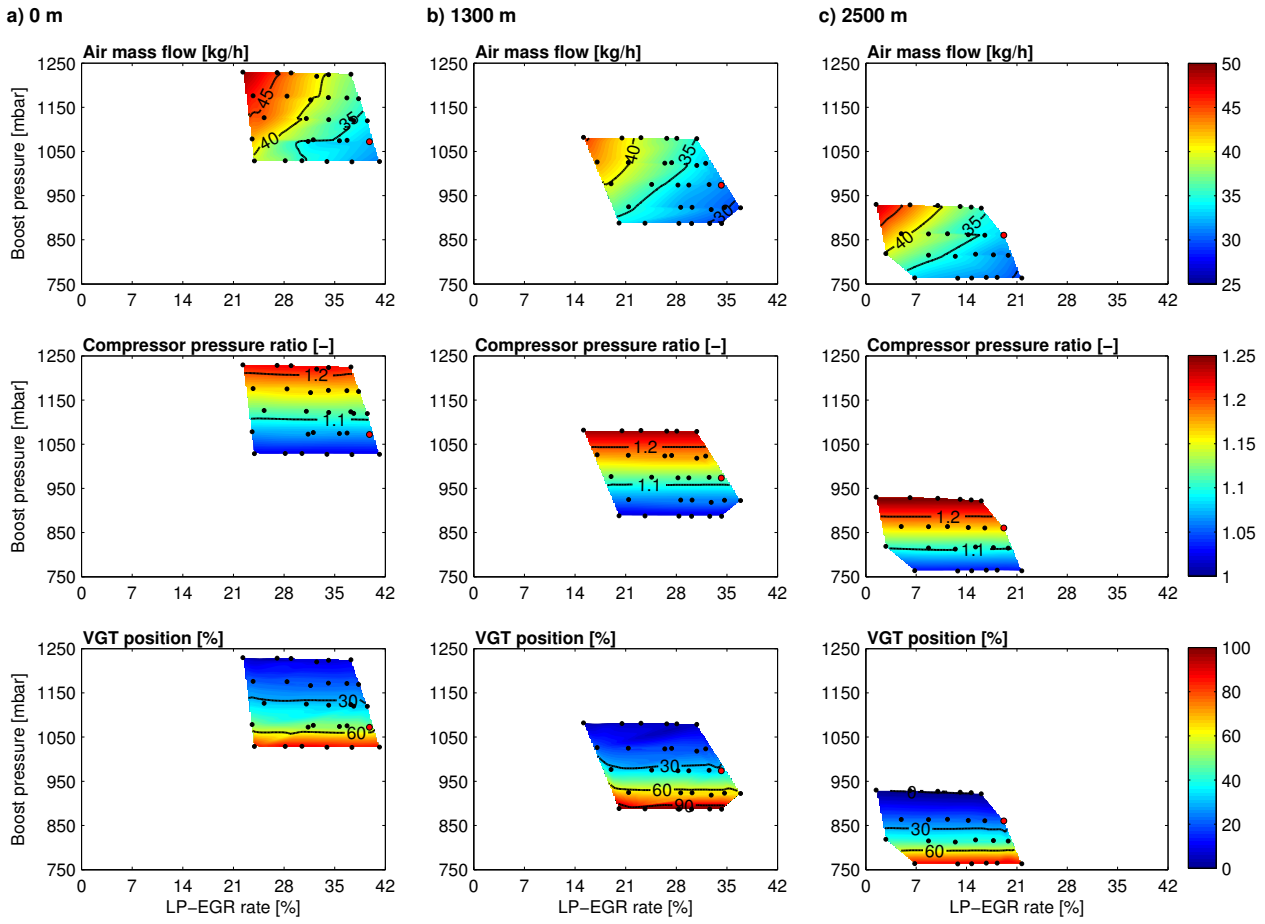

Figure 2. Air mass flow, compressor pressure ratio and VGT position corresponding to 1250 rpm & 3 bar at 25°C as a function of the altitude at: (a) 0 m, (b) 1300 m and (c) 2500 m.

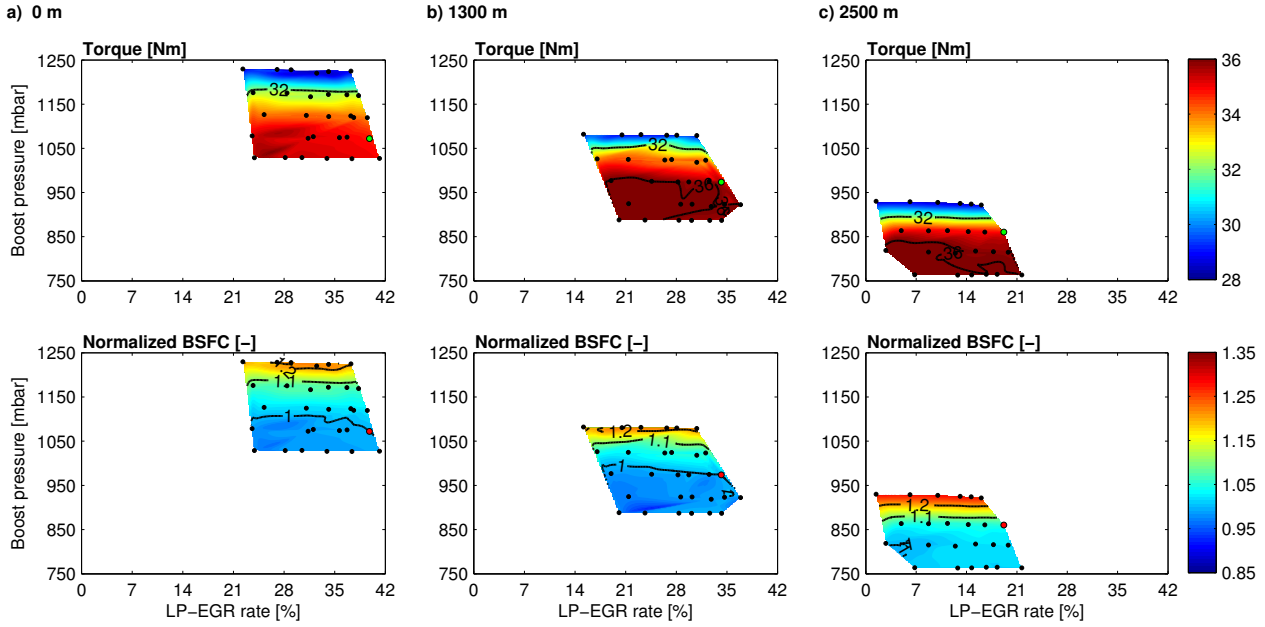

Figure 3. Engine torque and normalized BSFC corresponding to 1250 rpm & 3 bar at 25°C as a function of the altitude at: (a) 0 m, (b) 1300 m and (c) 2500 m.

However, the VGT outlet temperature reached its maximum at the minimum boost pressure, i.e. open VGT. Despite the highest VGT inlet temperature being produced at maximum boost pressure, the resulting high expansion ratio gave as a result a low outlet temperature. By contrast, opener VGT positions provided the expansion ratio convergence towards 1. Consequently, the temperature drop across the VGT was

highly reduced and the VGT outlet temperature remained the highest regardless the altitude and LP-EGR rate.

The main trends observed at 1250 rpm & 3 bar were confirmed in additional operating points. Figure 5 represents the normalized BSFC and VGT outlet temperature corresponding to 2000 rpm & 6 bar and 3000 rpm & 2 bar at 25°C in ambient temperature. In these plots, the focus is directly put on the comparison between sea-level and 2500 m operation, whose contours are plotted together. A relevant difference is observed for these two operating points in baseline altitude operating points (coloured dots on contours) with respect to 1250 rpm & 3 bar. The serial calibrated boost pressure was increased from sea-level to 2500 m by closing further the VGT. As a result, the BSFC sharply increased with respect to sea-level case with a minor benefit in VGT outlet temperature. However, these settings can be optimized, both at sea-level and extreme altitude operation.

Again, operating at lower boost pressure by opening the VGT led to an increase of the VGT outlet temperature regardless the LP-EGR rate, because of the increase of VGT inlet temperature (higher equivalence ratio) and very low expansion ratio. This increase was above 40°C at sea-level for both 2000 rpm & 6 bar as 3000 rpm & 2 bar. At 2500 m in driving altitude, the benefit was lower. The VGT outlet temperature increased $\sim$ 20 °C at 3000 rpm & 2 bar but was kept at 2000 rpm & 6 bar in the particular case of the serial calibration, i.e. reduction in boost pressure keeping the maximum LP-EGR rate. This was due to the serial calibration represented a singularity demanding a high VGT closing leading to both high pumping losses (extremely high spot in BSFC) and VGT outlet temperature due to the poor VGT efficiency. This is noticed by the high dependence of both BSFC and VGT outlet temperature on the LP-EGR at the baseline boost pressure. In fact, the decrease of the LP-EGR rate at this pressure provided the same trends as observed in other operating conditions. Regarding BSFC, sea-level operation was almost unresponsive in both operating points. However, the benefits at 2500 m were evident, especially at 3000 rpm & 2 bar due to the inherent poor efficiency and sensitivity to settings of the very low engine loads. In this point the BSFC was reduced around 25% as the boost pressure was reduced. The benefit also existed at 2000 rpm & 6 bar, reducing the BSFC above 15% from the baseline settings.

The results of the three tested engine operating points were completed with the same parametric studies as a function of altitude, boost pressure and LP-EGR at 45°C and -10°C in ambient temperature. The results, which, for the sake of brevity, are summarized in Figures 11 and 12 respectively in Appendix , support all the trends found at standard temperature: benefits from low boost pressure at low engine load operation in terms of simultaneous optimization of BSFC and aftertreatment warmup conditions. In addition, the determination of the optimal LP-EGR rate resulted also independent of these criteria and only limited by air mass flow management.

Pollutant emissions

Figure 6 represents the engine-out NO_x emission and opacity corresponding to the three tested points as function of the boost pressure and LP-EGR rate. In particular, the plots include the comparison between the results at sea-level and 25°C and those at 2500 m and -10°C, representing a standard versus an extreme ambient condition.

As expected, the engine-out NO_x emission were mainly governed by the LP-EGR rate. Nonetheless, the boost pressure also had a relevant weight in very low load cases, as 1250 rpm & 3 bar and 3000 rpm & 2 bar, particularly at high boost pressure and low LP-EGR rates in tests at -10°C. This dependence disappeared progressively as the LP-EGR rate and engine load increased, as observed in Figure 6(b) corresponding to 2000 rpm & 6 bar. In parallel, the sensitivity to the ambient temperature was also captured in every engine point, with lower NO_x emissions at -10°C despite the low LP-EGR rate influenced by a lower equivalence ratio in those conditions. As a general trend, imposing low boost pressure resulted beneficial (or neutral) in this operating range to reduce the engine-out NO_x emission along with increasing LP-EGR, obtaining synergy with minimum BSFC and maximum aftertreatement inlet temperature regardless the ambient condition. Despite the lower air mass flow as the boost pressure was decreased, the low level of the equivalence ratio made its increase not responsible of any NO_x emission variation. By contrast, the NO_x emission decreased at constant LP-EGR, as mainly observed in points 1250 rpm & 3 bar (Figure 6(a)) and 3000 rpm & 2 bar (Figure 6(c)), as the boost pressure did. This response was attributed to the in-cylinder temperature decay related to the combustion delay, which was in turn promoted by the ignition delay produced by the poorer mixing ratio as the boost pressure was decreased. Figure 7 represents how the crank angle at 10% of burned fuel mass (CA10) was progressively increased as the boost decreased.

As regards soot emission, which is depicted in the bottom row of Figure 6, the opacity was kept very low in all cases ($<$ 3%), being comparable at both ambient conditions. The soot dependence on the LP-EGR rate was only noticed at 2000 rpm & 6 bar (Figure 6(b)) in sea-level case. This was the only point in which the soot emission showed some sensitivity to the LP-EGR rate. Nevertheless, the low opacity and its minor variation as the boost pressure was decreased even at maximum LP-EGR rate (from 10% to 15%) in this case, besides the results corresponding to other points, contribute to advocate for low boost pressure settings at low engine load conditions.

Figure 8 illustrates the engine-out CO emissions and their conversion efficiency as a function of the boost pressure and LP-EGR rate. An engine operating point is represented in every column comparing sea-level and 25°C with 2500 m and -10°C as ambient boundaries. The engine-out CO emission was mainly dependent on LP-EGR rate at sea-level case, with an increase as the LP-EGR rate did in the three operating points, i.e. in trade-off with NO_x emission. In addition, sensitivity to the boost pressure also appeared at high LP-EGR rate producing the maximum engine-out CO emission at minimum boost pressure. Opposite, the main dependence moved to boost pressure at cold high altitude, along with a lower CO emission related to the lower LP-EGR rate. Nevertheless, the engine-out CO emission dependence on boost pressure in cold ambient resulted a function of the operating point, showing an increase with boost pressure in

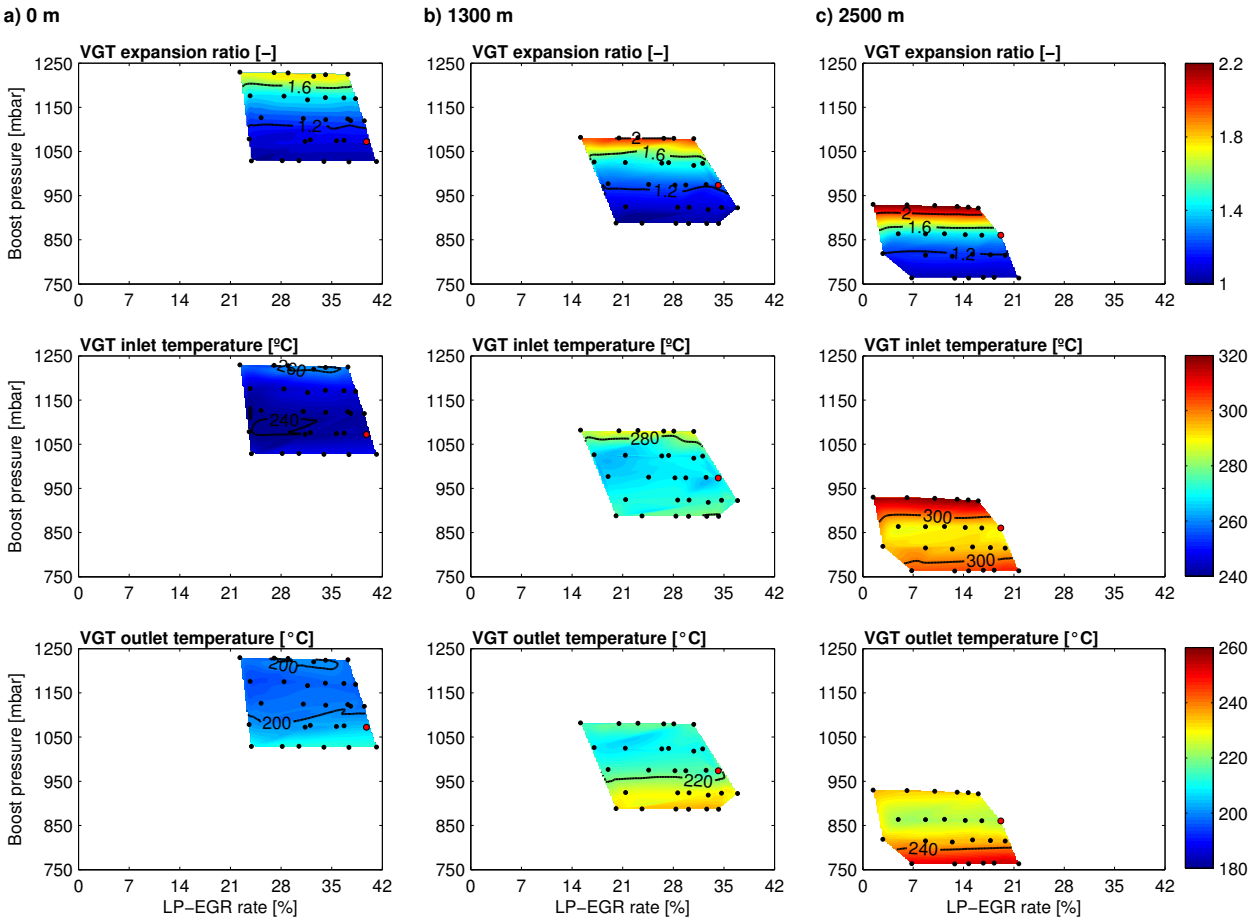

Figure 4. VGT expansion ratio, inlet temperature and outlet temperature corresponding to 1250 rpm & 3 bar at 25°C as a function of the altitude, boost pressure and LP-EGR rate at: (a) 0 m, (b) 1300 m and (c) 2500 m.

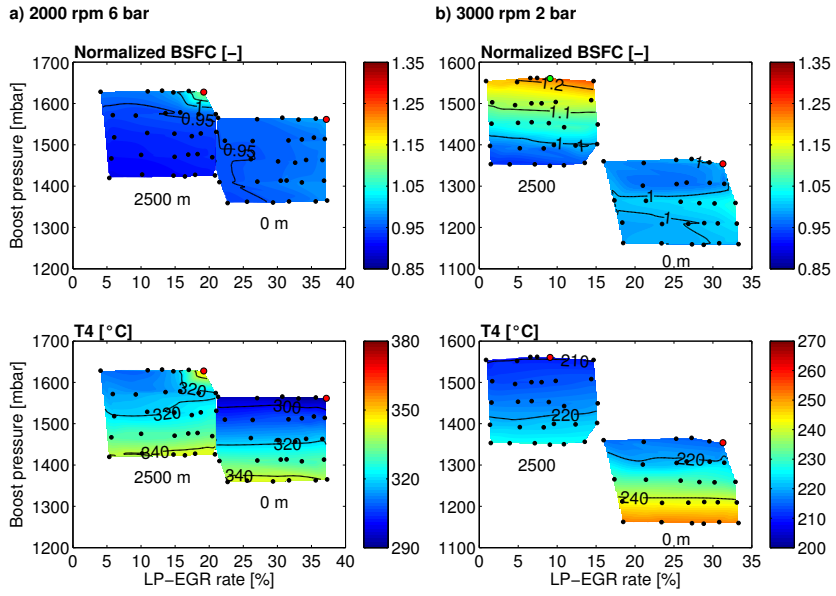

Figure 5. Normalized BSFC and VGT outlet temperature at 25°C in ambient temperature as a function of the altitude, boost pressure and LP-EGR rate for: (a) 2000 rpm & 6 bar and (b) 3000 rpm & 2 bar.

point 1250 rpm & 3 bar (Figure 8(a)), decrease in point 3000 rpm & 2 bar (Figure 8(c)) and no sensitivity in point 2500 rpm & 6 bar (Figure 8(b)). According to these results, the general trend was a slight increase of the engine-out CO emissions in the region of interest, i.e. minimum boost pressure to increase the VGT outlet temperature combined with minimum BSFC and maximum LP-EGR rate to minimize NO_x emission, with respect to the baseline operating points.

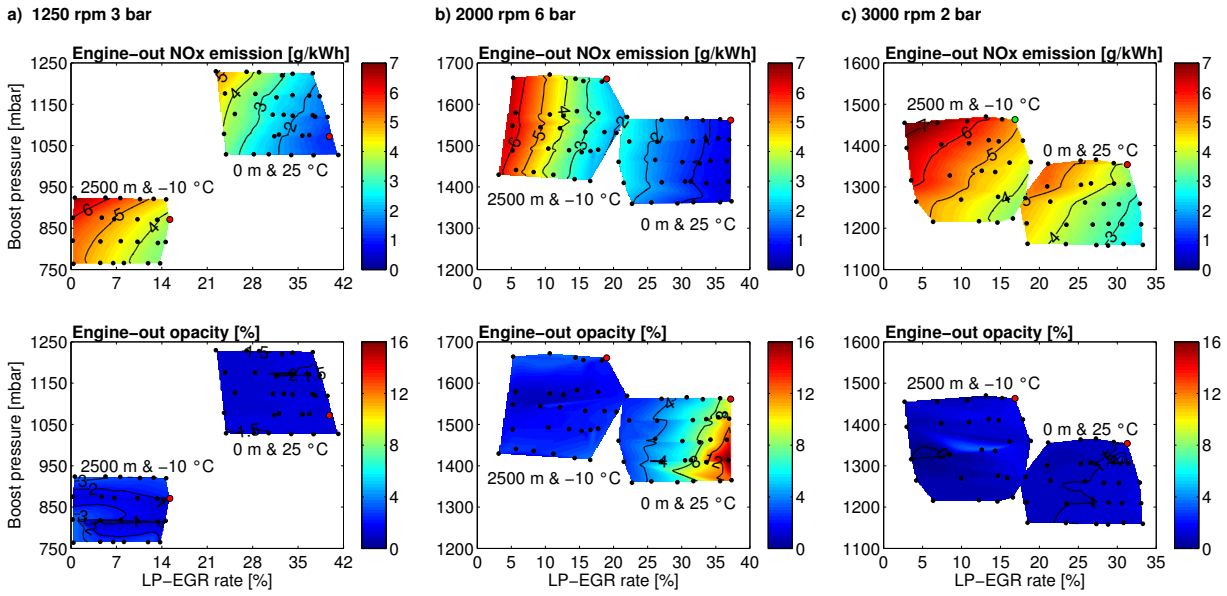

Figure 6. Engine-out NO_x emission and opacity as a function of the boost pressure and LP-EGR rate for sea-level at 25°C and 2500 m at -10°C for: (a) 1250 rpm & 3 bar, (b) 2000 rpm & 6 bar and (c) 3000 rpm & 2 bar.

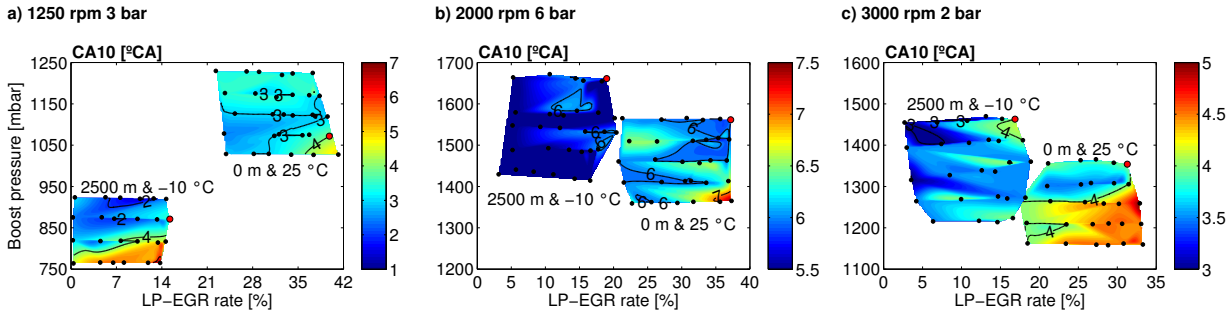

Figure 7. CA10 as a function of the boost pressure and LP-EGR rate for sea-level at 25°C and 2500 m at -10°C for: (a) 1250 rpm & 3 bar, (b) 2000 rpm & 6 bar and (c) 3000 rpm & 2 bar.

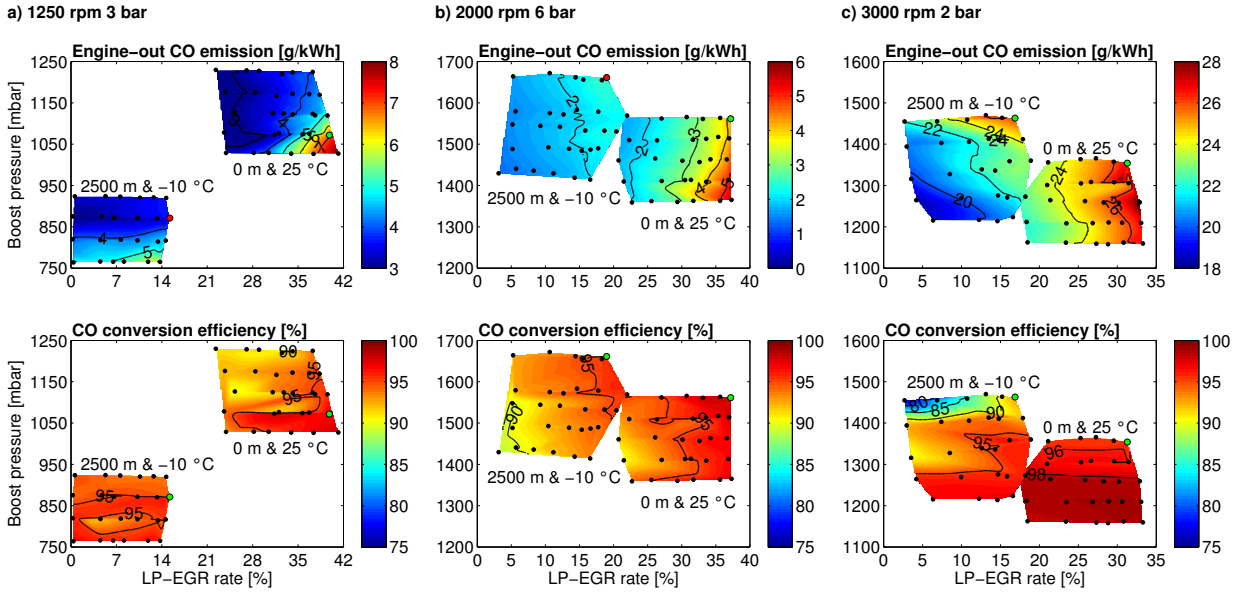

Figure 8. Engine-out CO emission and CO conversion efficiency as a function of the boost pressure and LP-EGR rate for sea-level at 25°C and 2500 m at -10°C for: (a) 1250 rpm & 3 bar, (b) 2000 rpm & 6 bar and (c) 3000 rpm & 2 bar.

The CO conversion efficiency is shown in the bottom row of Figure 8 for every operating point. The CO conversion efficiency yielded high values in agreement with VGT

outlet temperatures above 190°C for all cases, as shown in Figure 12 even for the most limiting ambient temperature (-10°C). It resulted in above 90% conversion efficiency with the only exception of cold altitude operation at 3000 rpm & 2 bar for high boost pressure and low LP-EGR rate settings. In this region, the CO conversion efficiency dropped to 80% evidencing sensitivity to the combination of the lowest VGT outlet temperature (Figure 12) and the maximum ATS mass flow (the lowest residence time), which is represented in Figure 9. This last magnitude was governed by the highest air mass flow due to maximum boost pressure and minimum LP-EGR rate, which in turn led to maximum volumetric efficiency. Regarding the region of interest, the CO conversion efficiency showed its maximum, above 96%, in the three operating points for all ambient boundaries and compensated the slight increase in engine-out CO emission.

Similar results were obtained concerning HC abatement, as represented in Figure 10. The upper row shows the engine-out HC emissions. These were kept very low with just certain trend to increase as the LP-EGR rate did as a main rule. However, the lower HC reactivity in comparison to CO at medium-high temperature, where the HC adsorption on zeolites becomes negligible[33], gave as a result a more marked trend in HC conversion efficiency, which is depicted for every operating point in the bottom row of Figure 10.

As observed in column (a) of Figure 10, the HC conversion efficiency at 1250 rpm & 3 bar showed the major variability within the tested window at sea-level and 25°C in ambient temperature. For this case, the HC conversion efficiency is clearly governed by the boost pressure. Its decrease led to higher residence time, due to the exhaust mass flow decrease (Figure 9), and to higher temperature (VGT outlet temperature in Figure 4). Consequently, the HC conversion efficiency increased as the boost pressure was decreased. This was the case with the highest sensitivity due to the temperature range $(190 - 210°C)$ around the light-off temperature[17]. This behaviour was also found in cold altitude operation. In this case, the residence time of the gas within the catalyst increased due to the lower boost pressure (lower exhaust mass flow) and the temperature moved to a higher range from 195 to $\sim 220°C$ (Figure 4). As a result, the HC conversion efficiency increased with respect to warm sea-level conditions. It varied from 65% at the highest boost pressure to 85% at the lowest one, corresponding to the maximum residence time and VGT outlet temperature.

Similar results can be observed at 2000 rpm & 6 bar (Figure 10(b)) and 3000 rpm & 2 bar (Figure 10(c)), with clear trend to HC conversion efficiency increase as the boost pressure decreased, favoured by the temperature and residence time, and regardless the LP-EGR rate. As the CO case, despite the slight increase in engine-out HC emissions when applying this strategy, the conversion efficiency was also benefited, offsetting the drawbacks related to the optimal BSFC and NO_x emission calibration.

Summary and conclusions

An experimental study on the impact of extreme ambient boundaries defined by the driving altitude (sea-level to 2500 m) and ambient temperature (-10 to 45°C on the performance and emissions at low load of a state-of-the-art engine was conducted. In particular, the effect of the boost pressure and the LP-EGR rate was analysed, with focus on the fuel consumption and the exhaust temperature. The results highlighted that minimum specific fuel consumption can be obtained along with the highest VGT outlet temperature benefiting aftertreatment warmup stretegies. To reach them, the target boost pressure should be decreased towards maximum VGT opening without dependence on the LP-EGR rate, i.e. no limitations for NO_x emission control. These trends were common in the three analysed points ranging from low to high speed and 2 to 6 bar BMEP. Neither the variation of altitude nor ambient temperature affected these calibration guidelines although more potential benefits on specific fuel consumption were found as the altitude increased. The reasons for the synergy between fuel consumption and exhaust temperature after the VGT expansion was found in the combination of several processes. On the one hand, the VGT opening contributed to decrease the pumping losses. On the other hand, the low expansion ratio provided the maximum VGT outlet temperature taking advantage of the very high VGT inlet temperature resulting from the higher equivalence ratio with these boost settings.

The proposed guidelines for air management calibration were also supported by the trends in the pollutants emissions and the catalyst performance. The serial calibrated LP-EGR rate, which was the highest tested value for every altitude and ambient temperature, resulted compatible with low boost pressure setting. This combination led the engine-out NOx emission to decrease with respect to the baseline one, being independent of the ambient boundary. Furthermore, only an increase of the NOx emission in altitude operation with respect to sea-level, which was caused by the LP-EGR rate decrease, was remarkable. This EGR reduction was required to provide the engine with similar fresh air mass flow as at sea-level operation.

The reduction of the NOx emission did not shown any relevant impact on soot. It remained almost constant with respect to serial engine calibration mostly due to the low equivalence ratio, despite of its increasing fashion with boost pressure reduction and LP-EGR rate increase. By contrast, the engine-out CO and HC emissions were slighly increased with these stretegies, as a main trend, showing higher sensitivity to the equivalence ratio increase. Despite of this negative impact, the increase of CO and HC emission wase restrained, keeping the emissions in the same order of magnitude as the baseline operating point at every altitude and ambient temperature. In fact, these slight increments were offset by the catalyst conversion efficiencies, which reached their maximum values at the lowest boost pressure and highest LP-EGR rates as a result of the higher exhaust temperature and catalyst residence time.

Acknowledgements

The Ph.D. student Bárbara Diesel has been funded by a grant from the Government of Generalitat Valenciana with reference ACIF/2018/109.

References

1. Joshi A. Review of vehicle engine efficiency and emissions. SAE Technical Paper 2020-01-0352, 2020.

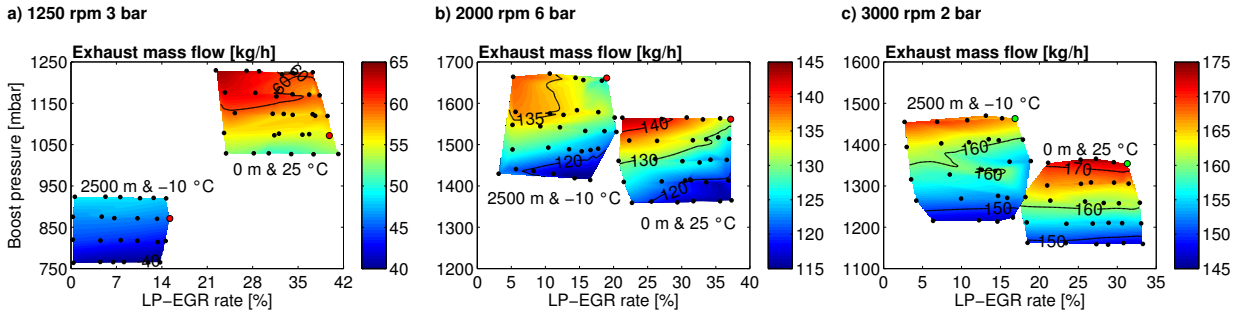

Figure 9. ATS mass flow as a function of the boost pressure and LP-EGR rate for sea-level at 25°C and 2500 m at -10°C for: (a) 1250 rpm & 3 bar, (b) 2000 rpm & 6 bar and (c) 3000 rpm & 2 bar.

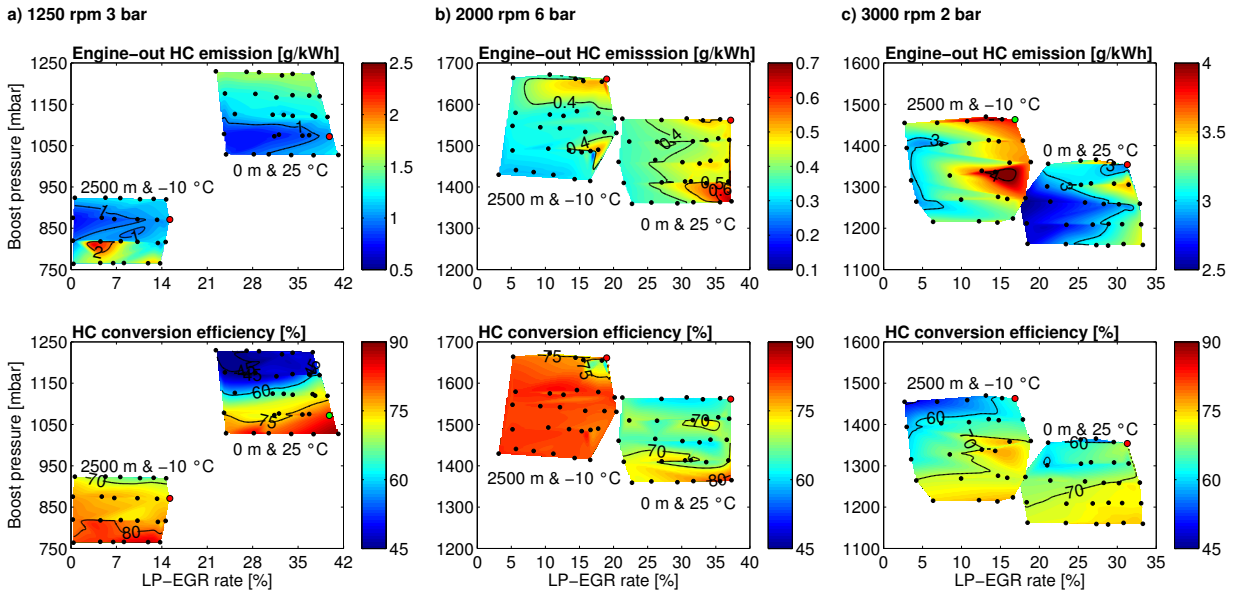

Figure 10. Engine-out HC emission and HC conversion efficiency as a function of the boost pressure and LP-EGR rate for sea-level at 25°C and 2500 m at -10°C for: (a) 1250 rpm & 3 bar, (b) 2000 rpm & 6 bar and (c) 3000 rpm & 2 bar.

2. European Commission. *Development of post-Euro 6/VI emission standards for cars, vans, lorries and buses.*, Ref. Ares no. 1800668, 2020.
3. Claßen J, Pischinger S, Krysmon S, Sterlepper S, Dorscheidt F, Doucet M, Reuber C, Görgen M, Scharf J, Nijs M, and Thewes SC. Statistically supported real driving emission calibration: Using cycle generation to provide vehicle-specific and statistically representative test scenarios for Euro 7. *Int J Engine Res* 2020; 21(10): 1783-1799, DOI:10.1177/1468087420935221.
4. Serrano JR, Piqueras P, Abbad A, Tabet R, Bender S and Gómez J. Impact on reduction of pollutant emissions from passenger cars when replacing Euro 4 with Euro 6d diesel engines considering the altitude influence. *Energies* 2019; 12: 1278, DOI:10.3390/en12071278.
5. Luján JM, Climent H, García-Cuevas LM and Moratal A. Pollutant emissions and diesel oxidation catalyst performance at low ambient temperatures in transient load conditions. *Appl Therm Eng* 2018; 129: 1527–1537, DOI:10.1016/j.applthermaleng.2017.10.138.
6. Ko J, Jin D, Jang W, Myunga CL, Kwon S and Park S. Comparative investigation of NO_x emission characteristics from a Euro 6-compliant diesel passenger car over the NEDC and WLTC at various ambient temperatures. *Appl Energy* 2018; 187: 652–662, DOI:10.1016/j.apenergy.2016.11.105.
7. Galindo J, Navarro R, Tarí D and Moya F. Development of an experimental test bench and a psychrometric model for assessing condensation on a low-pressure exhaust gas recirculation cooler. *Int J Engine Res* 2021; 22(5): 1540–1550, DOI: 10.1177/1468087420909735.
8. Galindo J, Piqueras P, Navarro R, Tarí D and Meano CM. Validation and sensitivity analysis of an in-flow water condensation model for 3D-CFD simulations of humid air streams mixing. *Int J Therm Sci* 2019; 136: 410–419, DOI: 10.1016/j.ijthermalsci.2018.10.043.
9. Galindo J, Dolz V, Monsalve-Serrano J, Bernal MA and Odillard L. Advantages of using a cooler bypass in the low-pressure exhaust gas recirculation line of a compression ignition diesel engine operating at cold conditions. *Int J Engine Res* 2021; 22(5): 1624–1635, DOI: 10.1177/1468087420914725.
10. Luján JM, Climent H, Ruiz S and Moratal A. Influence of ambient temperature on diesel engine raw pollutants and fuel consumption in different driving cycles. *Int J Engine Res* 2019; 20(8-9): 877–888, DOI:10.1177/1468087418792353.
11. Piqueras P, García A, Monsalve-Serrano J and Ruiz MJ. Performance of a diesel oxidation catalyst under diesel-gasoline reactivity controlled compression ignition combustion

conditions. *Energy Convers Manag* 2019; 196: 18–31, DOI:10.1016/j.enconman.2019.05.111.
12. Faria MV, Varella RA, Duarte GO, Farias TL and Baptista PC. Engine cold start analysis using naturalistic driving data: City level impacts on local pollutants emissions and energy consumption. *Sci Total Environ* 2018; 630: 544–559, DOI:10.1016/j.scitotenv.2018.02.232.
13. Ko J, Son J, Myung C and Park S. Comparative study on low ambient temperature regulated/unregulated emissions characteristics of idling light-duty diesel vehicles at cold start and hot restart. *Fuel* 2018; 233: 620–631, DOI:10.1016/j.fuel.2018.05.144.
14. Szedlmayer M and Kweon C. Effect of altitude conditions on combustion and performance of a multi-cylinder turbocharged direct injection diesel engine. SAE Technical Paper 2016-01-0742, 2016, DOI:10.4271/2016-01-0742.
15. Bermúdez V, Serrano JR, Piqueras P, Gómez J and Bender S. Analysis of the role of altitude on diesel engine performance and emissions using an atmosphere simulator. *Int J Engine Res* 2017; 18(1-2): 105–117, DOI:10.1177/1468087416679569.
16. Serrano JR, Piqueras P, Sanchis EJ and Diesel B. A modelling tool for engine and exhaust aftertreatment performance analysis in altitude operation. *Results in Engineering* 2019; 4: 100054, DOI:10.1016/j.rineng.2019.100054.
17. Serrano JR, Piqueras P, Sanchis EJ and Diesel B. Analysis of the driving altitude and ambient temperature impact on the conversion efficiency of oxidation catalysts. *Appl Sci* 2021; 11(3): 1283, DOI:10.3390/app11031283.
18. Wang X, Ge Y, Yu L and Feng X. Effects of altitude on the thermal efficiency of a heavy-duty diesel engine. *Energy* 2013; 59: 543–548, DOI:10.1016/j.energy.2013.06.050.
19. Giraldo M and Huertas JI. Real emissions, driving patterns and fuel consumption of in-use diesel buses operating at high altitude. *Transp Res D* 2019; 77: 21–36, DOI:10.1016/j.trd.2019.10.004.
20. Ramos A, García-Contreras R and Armas O. Performance, combustion timing and emissions from a light duty vehicle at different altitudes fueled with animal fat biodiesel, GTL and diesel fuels. *Appl Energy* 2016; 182: 507–517, DOI:10.1016/j.apenergy.2016.08.159.
21. Zervas E. Impact of altitude on fuel consumption of a gasoline passenger car. *Fuel* 2011; 90(6): 2340–2342, DOI:10.1016/j.fuel.2011.02.004.
22. Wang Y, Ge Y, Wang J, Wang X, Yin H, Hao L and Tan J. Impact of altitude on the real driving emission (RDE) results calculated in accordance to moving averaging window (MAW) method. *Fuel* 2020; 277: 117929, DOI:10.1016/j.fuel.2020.117929.
23. Yu L, Ge Y, Tan J, He C, Wang X, Liu H, Zhao W, Guo J. Fu G, Feng X and Wang X. Experimental investigation of the impact of biodiesel on the combustion and emission characteristics of a heavy duty diesel engine at various altitudes. *Fuel* 2014; 115: 220–226, DOI:10.1016/j.fuel.2013.06.056.
24. Wang H, Ge Y, Hao L, Xu X, Tan J, Li J, Wu L, Yang J, Yang D, Peng J, Yang J and Yang R. The real driving emission characteristics of light-duty diesel vehicle at various altitudes. *Atmos Environ* 2018; 191: 126–131, DOI:10.1016/j.atmosenv.2018.07.060.
25. Yang M, Gu Y, Deng K, Yang Z and Zhang Y. Analysis on altitude adaptability of turbocharging systems for a heavy-duty diesel engine. *Appl Therm Eng* 2018; 128: 1196 – 1207, DOI:10.1016/j.applthermaleng.2017.09.065.
26. Thompson AT. *The effect of altitude on turbocharger performance parameter for heavy duty diesel engines: experiments and GT-Power modeling*. Master Thesis, Colorado State University, US, 2014.
27. Wang J, Shen L, Bi Y and Lei J. Modeling and optimization of a light-duty diesel engine at high altitude with a support vector machine and a genetic algorithm. *Fuel* 2021; 285: 119137, DOI:10.1016/j.fuel.2020.119137.
28. Galindo J, Serrano JR, Piqueras P and Gómez J. Description and performance analysis of a flow test rig to simulate altitude pressure variation for internal combustion engines testing. SAE Technical Paper 2014-01-2582, 2014, DOI:10.4271/2014-01-2582.
29. Galindo J, Serrano JR, Piqueras P and Gómes J. Description and performance analysis of a flow test rig to simulate altitude pressure variation for internal combustion engines testing. *SAE Int J Engines* 2014; 7(4): 1686–1696, DOI:10.4271/2014-01-2582.
30. Broatch A, Bermúdez V, Serrano JR, Tabet R, Gómez J and Bender S. Analysis of passenger car turbocharged diesel engines performance when tested at altitude and of the altitude simulator device used. *J Eng Gas Turbines Power* 2019; 141(8): 081017, DOI:10.1115/1.4043395.
31. Desantes JM, Galindo J, Payri F, Piqueras P and Serrano JR. *Device for atmosphere conditioning for testing combustion engines, and associated method and use*. Patent WO 2015/110683 A1, 2015.
32. Desantes JM, Galindo J, Payri F, Piqueras P and Serrano JR. *Device for conditioning the atmosphere in test of alternative internal combustion engines, method and use of said device*. Patent WO 2016/116642 A1, 2016.
33. Piqueras P, Ruiz MJ, Herreros JM, Tsolakis A. Sensitivity of pollutants abatement in oxidation catalysts to the use of alternative fuels. *Fuel* 2021; Accepted for publication.

Nomenclature

ATS	aftertreatment system
BMEP	break mean effective pressure
BSFC	brake specific fuel consumption
DOC	diesel oxidation catalyst
ECU	engine control unit
EGR	exhaust gas recirculation
LNT	lean NO_x trap
LP-EGR	low pressure exhaust gas recirculation
MEDAS	multifunctional efficient dynamic altitude simulator
NEDC	new European driving cycle
PM	particulate matter
RDE	real driving emissions
VGT	variable geometry turbine
WCAC	water charge air cooler
WLTC	worldwide harmonized light vehicles test cycle

Appendix. BSFC and VGT outlet temperature at additional operating points

The trends in normalized BSFC and VGT outlet temperature as a function of the ambient boundaries for the parametric studies described in Section is completed next. Figure 11 represents the normalized BSFC and VGT outlet temperature

for every engine operating point at sea-level and 2500 m corresponding to 45°C in ambient temperature. Complementary, Figure 12 provides the equivalent results for cold ambient conditions (-10°C).

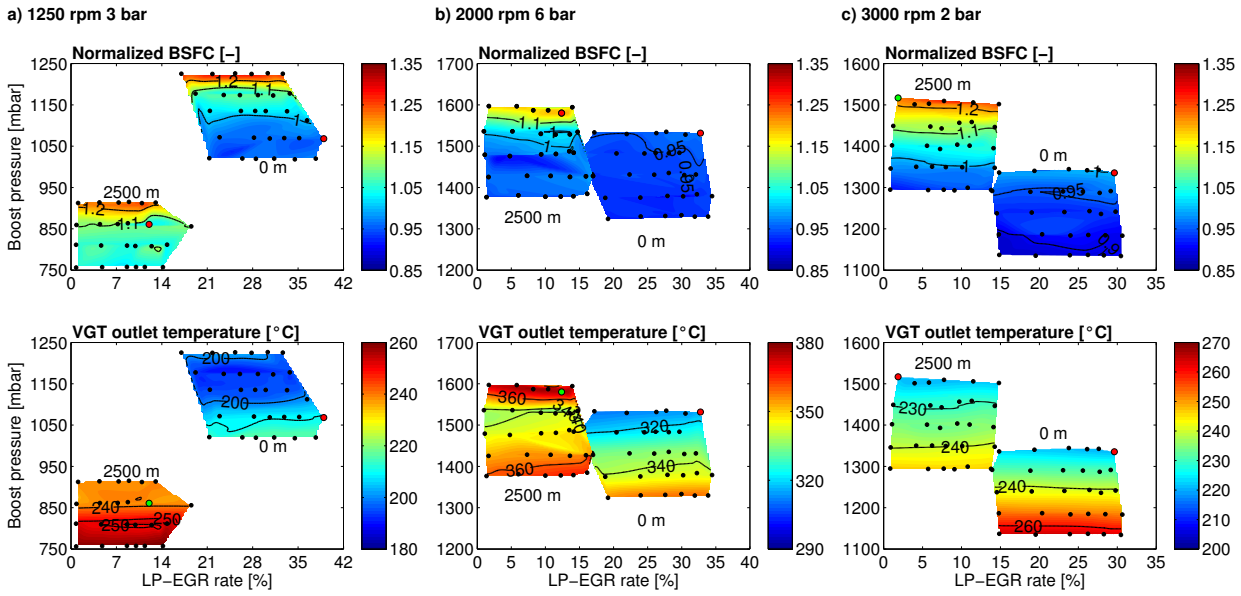

Figure 11. Normalized BSFC and VGT outlet temperature at 45°C in ambient temperature as a function of the altitude, boost pressure and LP-EGR rate at: (a) 1250 rpm & 3 bar, (b)2000 rpm & 6 bar and (c) 3000 rpm & 2 bar.

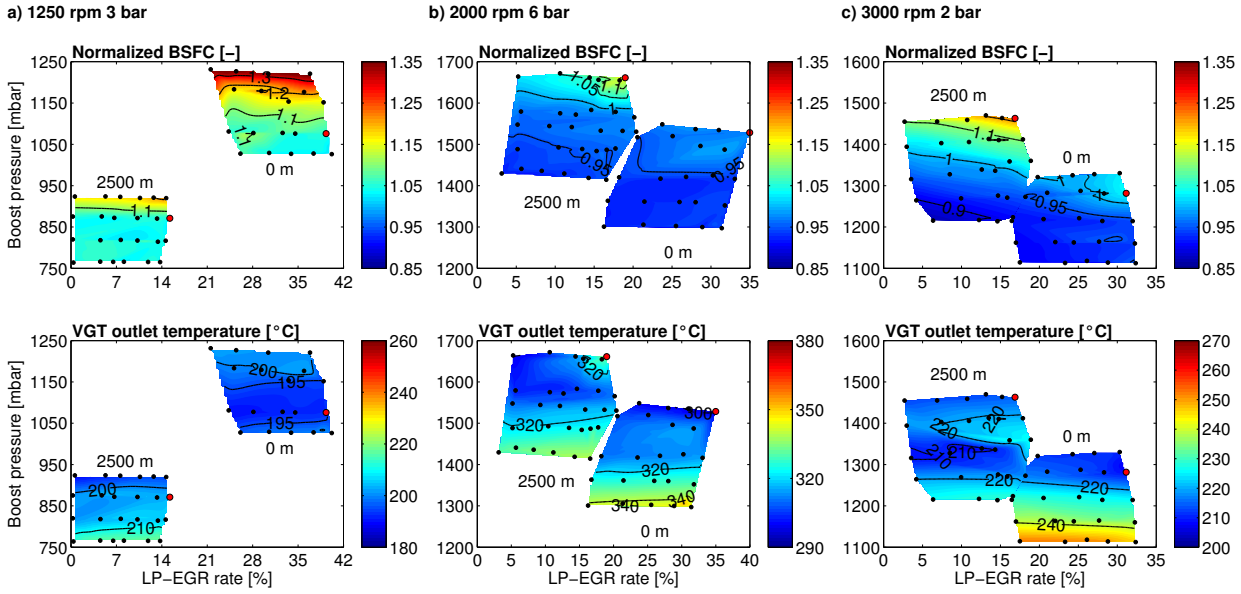

Figure 12. Normalized BSFC and VGT outlet temperature at -10°C in ambient temperature as a function of the altitude, boost pressure and LP-EGR rate at: (a) 1250 rpm & 3 bar, (b)2000 rpm & 6 bar and (c) 3000 rpm & 2 bar.